Published in final edited form as:
Biomaterials. 2015 March ; 44: 55–70. doi:10.1016/j.biomaterials.2014.12.009.

Protease-degradable PEG-maleimide coating with on-demand release of IL-1Ra to improve tissue response to neural electrodes

Stacie M. Gutowski[1,2], **James T. Shoemaker**[1,2], **Kellie L. Templeman**[2,3], **Yang Wei**[4], **Robert A. Latour Jr.**[4], **Ravi V. Bellamkonda**[1,2], **Michelle C. LaPlaca**[1,2], and **Andrés J. García**[2,3,*]

[1]Wallace H. Coulter Department of Biomedical Engineering, Georgia Institute of Technology, Atlanta, GA

[2]Petit Institute for Bioengineering and Bioscience, Georgia Institute of Technology, Atlanta, GA

[3]Woodruff School of Mechanical Engineering, Georgia Institute of Technology, Atlanta, GA

[4]Department of Bioengineering, Clemson University, Clemson, SC

Abstract

Neural electrodes are an important part of brain-machine interface devices that can restore functionality to patients with sensory and movement disorders. Chronically implanted neural electrodes induce an unfavorable tissue response which includes inflammation, scar formation, and neuronal cell death, eventually causing loss of electrode function. We developed a poly(ethylene glycol) hydrogel coating for neural electrodes with non-fouling characteristics, incorporated an anti-inflammatory agent, and engineered a stimulus-responsive degradable portion for on-demand release of the anti-inflammatory agent in response to inflammatory stimuli. This coating reduces *in vitro* glial cell adhesion, cell spreading, and cytokine release compared to uncoated controls. We also analyzed the *in vivo* tissue response using immunohistochemistry and microarray qRT-PCR. Although no differences were observed among coated and uncoated electrodes for inflammatory cell markers, lower IgG penetration into the tissue around PEG +IL-1Ra coated electrodes indicates an improvement in blood-brain barrier integrity. Gene expression analysis showed higher expression of IL-6 and MMP-2 around PEG+IL-1Ra samples, as well as an increase in CNTF expression, an important marker for neuronal survival. Importantly, increased neuronal survival around coated electrodes compared to uncoated controls was observed. Collectively, these results indicate promising findings for an engineered coating to increase neuronal survival and improve tissue response around implanted neural electrodes.

[*]Corresponding Author: Andrés J. García, 315 Ferst Drive, IBB Building, Atlanta, GA 30332-0363, U.S.A., andres.garcia@me.gatech.edu.

Introduction

Neural electrodes are an important part of brain-machine interface devices that may one day restore functionality to patients with spinal cord injury, prosthetic limbs, and sensory impairments (1–4). However, the recording ability of the majority of electrodes fails within days to weeks after implantation (5), rendering the current technology inconsistent and unstable. While many modifications have been made to improve long-term neural electrode functionality, many issues still persist including acute and chronic inflammation, microglia and astrocyte recruitment, scar formation, and death of neurons surrounding the implanted electrode (6–10). In addition, microvasculature is compromised upon electrode implantation causing blood-brain barrier (BBB) breach. The severity of BBB breach is an important determinant in the long-term tissue response to implanted devices, with BBB breach causing increased inflammation and neuronal death as well as correlating with decreased electrode recording functionality (11, 12). This combination of responses will eventually cause the electrode to cease functioning.

Numerous electrode coatings have been developed to improve electrode performance as well as the *in vitro* and *in vivo* response to electrodes. Conductive coatings are a widely-tested option as they can improve the electrical performance of the electrode (13, 14). Combinations of poly(3,4-ethylenedioxythiophene)/poly(styrene sulfonate) (PEDOT/PSS) or polypyrrole (PPy) with a peptide-derivative from laminin have shown promising results to decrease impedance on the active sites of electrodes, making it easier for neuronal signals to reach the electrode surface (15–17). Additional research with PEDOT/PPy nanotubes showed improved electrical properties as well as improved neurite outgrowth on the electrode surface (18). Others have tried passive polymer coatings to reduce protein adsorption and cell adhesion on the electrode surface. Polyaniline-coated platinum electrodes (19) and low-protein binding polymer films on silicon electrodes (20) showed reduced protein adsorption, while PEG-NIPAm microgel coatings also showed reduced cell adhesion and cell spreading *in vitro* compared to unmodified controls (21). Poly(vinyl alcohol)/poly(acrylic acid) coatings reduce protein adsorption and astrocyte recruitment around the electrode site (22), while combination PEG/polyurethane coatings have reduced glial scarring and neuronal death around PEG/PU coated electrodes (23). Several groups have also investigated the effectiveness of incorporating bioactive factors into a coating. Bezuidenhout et al. demonstrated that loading dexamethasone into degradable and non-degradable PEG hydrogels improves tissue responses (24). Further studies showed reduced inflammatory response and increased neuronal survival with dexamethasone-releasing coatings (25–28). Dexamethsone treatments have also yielded reduced astrocytic response in an *in vivo* model (29, 30). Incorporating α-melanocyte stimulating hormone into a nitrocellulose coating on the electrode surface reduced LPS-stimulated nitrite production *in vitro* (31) and incorporation of TGF-β on a laminin coating yielded reduced astrocytic recruitment on the electrode surface compared to laminin alone, indicating a potential target for reducing astrocytic scar formation (32). Additionally, multi-functional coating approaches have attempted to address several problems simultaneously. Abidian and Martin incorporated slow-release dexamethasone into an alginate hydrogel with PEDOT functionalization to improve electrical impedance with promising release characteristics *in*

vitro (33), while Wadhwa et al. showed similar results with a polypyrrole coating and dexamethasone release *in vitro* (34). Potter et al. utilized a poly(vinyl alcohol) material to improve the mechanical characteristics of the electrode to reduce mechanical mismatch while also incorporating curcumin to mediate the inflammatory response (35) with promising results at 4 weeks post-implantation, but all improvements were lost by 12 weeks. Although there have been many attempts to improve electrode performance and tissue response, a solution has not been found that can address all problems associated with implanted neural electrodes.

Previous work from our group has shown that modifying the surface of an electrode with a non-fouling coating alone is not sufficient to reduce inflammatory cell recruitment or neuronal loss for electrodes implanted in the rat brain (21). These findings prompted us to re-engineer the coating to incorporate an anti-inflammatory agent into the non-fouling coating with the goal of reducing inflammation and neuronal loss in the surrounding tissue. Interleukin 1 (IL-1) is an important cytokine in the inflammatory cascade both in the brain and throughout the body, and the presence of IL-1 can promote production of additional cytokines in the inflammatory cascade. Interleukin-1 receptor antagonist (IL-1Ra) is a 17 kDa protein that has been implicated as an important mediator of inflammation in diseases and conditions that contain IL-1 as part of the inflammatory cascade (36, 37). In the central nervous system, IL-1Ra reduces inflammation in the spinal cord, and it is also implicated in the recovery process after brain ischemia as well as stroke (36, 37). IL-1Ra also has neuroprotective effects when released by microglia (38). Taub et al. examined the effects of IL-1Ra integrated into a laminin coating on neural electrodes and noted moderate improvement of the astrocyte response to the IL-1Ra-coated electrodes compared to uncoated controls, however no other cell types were analyzed (39). Additionally, IL-1Ra is already approved for use in humans as a therapeutic for other inflammatory conditions such as arthritis (36). Based on these data, we hypothesized that IL-1Ra is a suitable candidate as an immunomodulator to improve the tissue response to implanted neural electrodes.

Rather than simply adding IL-1Ra to the coating for passive release, we engineered an on-demand release characteristic to the coating. MMPs are up-regulated in many disease states and conditions that cause increased inflammatory response (40, 41), including neurodegenerative diseases (42), central nervous system injury (43–45) brain injury (46, 47), and around implanted neural electrodes (11, 48). Since MMPs are up-regulated in the inflammatory cascade in the brain, it is possible to utilize MMPs that are already present in the inflamed tissue to serve as the stimuli to break down a material, such as a hydrogel, that contains MMP-degradable motifs to release therapeutic agents. MMP-degradable hydrogels have been used for diverse applications including encapsulation of mesenchymal stem cells (49), fibroblasts (50, 51), vascular smooth muscle cells (52), drugs (53), and biomolecules such as RGD and VEGF (54–56). The MMP-degradable nature of these hydrogels allows for host cells to remodel the gels, allowing for cell ingrowth as well as release of any incorporated bioactive factors.

In the present study, we engineered a neural electrode coating with three essential components:

1. a protein adsorption- and cell adhesion-resistant PEG hydrogel;
2. incorporated anti-inflammatory IL-1Ra;
3. protease-sensitive crosslinkers for on-demand release of IL-1Ra in response to proteases which are up-regulated during inflammation.

We hypothesized that a coating comprising a protein adsorption/cell adhesion-resistant layer with controlled on-demand release of the anti-inflammatory agent IL-1Ra would improve the tissue response and neuronal survival near the implant-tissue interface.

Materials and Methods

PEG-maleimide Hydrogel Coating of Electrodes

Electrodes were purchased from NeuroNexus Technologies (CM16 A4×4-4mm-200-200-1250) and consist of a silicon substrate with iridium wires and active sites. Each electrode is 4-mm long with four active sites on each of four prongs, and each active site has an area of 1250 μm^2. In some instances, silicon wafers were used as a surrogate for the Si substrate of the electrodes. Silicon substrates were cleaned to remove contaminants using serial 5-min incubations in trichloroethylene (JT Baker), acetone (Sigma-Aldrich), and methanol (Sigma-Aldrich). Substrates were then rinsed with absolute ethanol (Decon Labs). The surface was functionalized using a silane-based adhesion layer grafted onto the silicon oxide layer of the electrode/wafer. Briefly, the substrates were incubated for 2 h in 2.5% silane-PEG-maleimide (Nanocs) in DMSO, then rinsed with absolute ethanol and PBS. Multi-treatment PEG-mal coatings were deposited using a dip-coating technique developed for this research. Silane-PEG-maleimide-modified samples were incubated in solution with crosslinking peptide, either GCRDGDQGIAGFDRCG (GDQ) or GCRDVPMSMRGGDRCG (VPM) (peptides were custom synthesized by AAPPTec), for 2 min, rinsed with PBS, incubated for 2 min in 20 kDa 4-arm PEG-maleimide (Laysan Bio), and rinsed with PBS (Fig. 1a). Alternating incubations in crosslinking peptide followed by PEG-maleimide were repeated to achieve the desired number of treatments per coating, with each set of peptide and PEG-maleimide considered as one complete treatment. For samples presenting only the PEG hydrogel (designated as PEG), the samples were coated with six treatments of PEG-maleimide and GDQ, whereas the coatings containing IL-1Ra (PEG+IL-1Ra) were coated with two treatments of PEG-maleimide and GDQ followed by four treatments of PEG-maleimide/IL-1Ra and VPM. Although the coatings do incorporate different crosslinkers, this hydrogel system with both crosslinkers has been extensively characterized by our lab and there are minimal differences in hydrogel structure. Coating deposition was verified by X-ray photoelectron spectroscopy (XPS). Coating thickness was analyzed by wet-cell ellipsometry of coatings on Si wafers. Ellipsometry measurements were performed using a GES5 variable angle spectroscopic ellipsometer (Sopra) and the accompanying GESPack software package. Briefly, a total of six spectra for at least two test points on each sample in deionized water were scanned from 350 nm to 800 nm at 10 nm intervals using an incident angle of 70°. The thickness of the coating was estimated from a model and determined using the regression method in Sopra's Winelli (ver. 4.08) software.

In Vitro Analysis of Cell Adhesion and Cytokine Release

Either uncoated or PEG-coated silicon wafers were placed in individual wells of a 96-well plate. The samples (n = 4 per group) were washed three times with 70% ethanol followed by three washes with sterile PBS. Mixed astrocyte and microglial cells (isolated from rat brains (57)) were added to each well at a density of 50,000 cells/cm^2. The samples were cultured in DMEM/F12 (Invitrogen) and 10% FBS (Invitrogen) at 37°C and 5% CO_2 for 24 h. Samples were stained with LIVE/DEAD stain (Invitrogen) and imaged with a 20X Apo Nikon objective (0.75 NA). Cell spread area on the electrode surface was measured using ImageJ software (NIH).

Uncoated, PEG, or PEG+IL-1Ra-coated samples (n = 4 per group) were placed in a 96-well plate and washed three times with 70% ethanol followed by three times with sterile PBS. Mixed astrocytes and microglia cells were seeded at a density of 30,000 cells/well in DMEM + N2 supplement (Life Technologies) in an ultra-low attachment cell culture plate. Cells were incubated overnight at 37°C and 5% CO_2 before rinsing the samples and transferring the samples to a new well. The samples were stimulated with 10 ng/ml granulocyte macrophage colony stimulating factor (GM-CSF) to promote cytokine secretion (20) and incubated for 48 h. Levels of IL-1β and TNF-α were analyzed using ELISA (R&D Systems).

IL-1Ra Release Characterization

Si wafer samples (n = 4 per group) were coated as described above. The samples were placed in a 96-well plate and washed three times with 70% ethanol followed by three washes with sterile PBS. The samples were incubated with supernatant from LPS-stimulated mixed glia cultures or naive media and supernatant samples were collected (and replaced by an equal volume of supernatant from LPS-stimulated mixed glia culture or media) at specified time points for analysis using an ELISA (R&D Systems).

Electrode Implantation

NIH guidelines for the care and use of laboratory animals (NIH Publication #85-23 Rev. 1985) were observed. All surgical procedures were approved by the Institutional Animal Care and Use Committee at the Georgia Institute of Technology. Male Sprague-Dawley rats (Charles River Laboratories, n = 15 per group (n = 8 for immunostaining, n = 7 for PCR)) weighing 200–300g were anesthetized with isofluorane. The surgical site was shaved and hair removed with Nair, then cleaned with isopropyl alcohol and chlorohexaderm before mounting the animal onto a stereotactic frame. Marcaine (0.15 mL of 0.5%) was injected subcutaneously at the site of incision. A midline incision 2–3 cm long was made in the scalp and the periosteum retracted to expose the cranium. Three 1 mm-diameter pilot holes were made around the skull, two posterior to bregma on either side of the midline and one anterior and right of bregma. A 4.7 mm stainless steel bone screw (Fine Science Tools 19010-00) was inserted into each of the pilot holes, with each screw penetrating the skull but leaving 1–2 mm of each screw head remaining out of the skull to serve as an attachment point for the headcap. The craniotomy for electrode insertion was made anterior to and left of bregma using a 2.7 mm trephine bit (Fine Science Tools 18004-27). The dura was resected and folded away from the insertion site. The electrode was held in the stereotactic frame above

the 2.7 mm hole and slowly lowered into the cortex, careful to avoid any large vasculature in the surgical area. Agarose gel (1.5% w/v, SeaKem) was filled into the opening around the electrode and dental acrylic (OrthoJet) was used to anchor the electrode assembly to the skull. The scalp incision was closed and triple-antibiotic ointment was applied to the wound. Each animal was given an injection of 0.03 mg/kg sustained release buprenorphine for pain relief and allowed to recover from anesthesia under a heat lamp. All animals were fully ambulatory post recovery and no complications were observed.

At 4 weeks the animal was anesthetized with ketamine/xylazine/acepromazine (50, 10, and 1.67 mg/kg body weight respectively). For samples used for histological sections (n = 8 per group), the animal underwent transcardial perfusion with 200 mL 0.4% papaverine HCl in 0.9% NaCl, followed by 50 mL of 0.9% NaCl, and 200 mL of 4% paraformaldehyde in phosphate buffer. After perfusion, the rat was decapitated and excess tissue removed from the skull before placing the intact skull into 4% paraformaldehyde overnight. The following day, the intact skull was moved to 30% sucrose in PBS. After one day in 30% sucrose, the skull cavity was opened and the brain was carefully removed. Any electrodes remaining in the brain were removed from the tissue before placing the whole brain into a 50 mL conical tube with 30% sucrose overnight until the brain sank to the bottom of the tube. Samples were then embedded in OCT and frozen using isopentane in liquid nitrogen. For samples to be used for qRT-PCR analysis (n = 7 per group), the animal was anesthetized with ketamine/xylazine/acepromazine prior to transcardial perfusion with 100 mL cold PBS followed by 100 mL 30% sucrose in PBS. Following perfusion, the rat was decapitated and the brain promptly removed from the skull. A 2-mm biopsy punch was used to remove brain samples which were immediately placed in RNAlater (Life Technologies) and stored at −20°C until analysis by qRT-PCR.

Immunostaining Evaluation

Samples were sectioned in 16-μm thick sections using a cryostat and stained for various cell markers as indicated in Table 1. All primary antibodies were visualized with AlexaFluor 488-conjugated secondary antibody (Invitrogen) and counterstained with DAPI for cell nuclei recognition. Upon completion of staining, all slides were imaged using a 10X Nikon objective (0.30 NA) and SPOT Advanced software (Diagnostic Instruments). Data obtained from *in vivo* studies were analyzed using MATLAB software (Mathworks) as previously described (21). A line was drawn manually along the boundary of the injury caused by the electrode and the intensity values were gathered starting at the boundary of the injury and moving 500 μm perpendicularly from the line. The average intensity was normalized to the intensity of the contralateral [background] image by utilizing point by point subtraction of the background staining (obtained from the corresponding contralateral uninjured hemisphere) from the injury image, taking into account the variation of field illumination. Each curve was fit to equation 1 and a five-parameter fit applied to each curve.

$$normalized\ intensity = intensity_1 * e^{-(x * decay(proximal))} + intensity_2 * e^{-(x * decay(distal))} + f. \quad \text{Eqn. 1}$$

This equation provides two intensity and decay parameters corresponding to the proximal steep decay in the intensity curve at distances corresponding to 0–100 μm (proximal to

electrode, parameters: intensity$_1$ and decay$_{proximal}$) followed by a second decay in the intensity curve at distances >100 μm from the edge of injury (distal to electrode, parameters: intensity$_2$ and decay$_{distal}$). Sample sections from each animal were used to generate independent intensity curves for each marker (GFAP, OX42/CD11b, ED1/CD68, IgG, CS56). A pilot study demonstrated no gross differences in inflammatory markers along the mid-shaft of the electrode, so all analyses were performed using sections at approximately 500 μm from the cortex surface. One tissue slice was analyzed per animal because pilot studies demonstrated that there are no differences in staining parameters between one vs. multiple sections per animal. The intensity curves for each individual animal were then combined and analyzed to obtain an inter-animal average per group for each marker at each time point. Analysis for NeuN staining utilized a similar methodology by analyzing cell staining starting at the scar and moving 500 μm away from the injury. Staining is analyzed by counting NeuN+ cells per 50 or 100 μm bin (7), as the staining for NeuN is either positive or negative for neuronal nuclei, with the number of positive cells indicating the number of neuronal nuclei in the analysis area.

Quantitative Reverse Transcriptase – Polymerase Chain Reaction (qRT-PCR)

Samples for qRT-PCR were stored in RNAlater buffer (Qiagen) until processing. Individual biopsy punch samples (2 mm diameter) from the electrode implantation site and the uninjured contralateral hemisphere were collected from each animal. Samples were placed in Qiazol (Qiagen) and homogenized using a Lab Gen 7 tissue homogenizer (Cole Palmer) for ~1 min. Tissue homogenate was placed in a QIAshredder column followed by total RNA extraction with the RNEasy MinElute Cleanup Kit (Qiagen). All RNA samples were tested for quality using a Nanodrop and had a 260/280 value of 2.0 or higher. Subsequent cDNA conversion was completed using the RT^2 First Strand Kit (Qiagen). Total cDNA, corresponding to mRNA expression, was analyzed using the Fluidigm BioMark system. Sixteen gene targets (Table 2) were analyzed to observe changes in inflammation as well as neural cell markers, and GAPDH was used as a housekeeping gene. The Ct values were normalized using ΔΔCt method (48), normalizing to the contralateral uninjured hemisphere and the housekeeping gene. Results are presented as fold change in gene expression compared to the uninjured contralateral hemisphere per group.

Statistical Analysis

Data presented are mean +/− standard error. All analyses were performed using GraphPad Prism 6.0. Statistical analyses for differences between thickness of multiple treatments of PEG hydrogel, *in vitro* cell adhesion, and cytokine release were performed using one-way ANOVA with Tukey's multiple comparison test. Statistical analysis of differences between PEG and PEG+IL-1Ra coating thickness was analyzed using an unpaired t-test. Curve fit parameters for immunostaining intensity curves were analyzed for normal distribution using the D'Agostino & Pearson normality test. As these parameters were found be not normally distributed, the curve-fit parameters were analyzed using a Kruskal-Wallis test with Bonferroni-Dunn's multiple comparison test to test for differences among groups. Analysis of NeuN data was performed using a 2-way repeated measures ANOVA with Tukey's multiple comparison test. PCR data was analyzed using a one-way ANOVA with Tukey's

multiple comparison to test for differences between groups. A p-value <0.05 was considered significant.

Results

Characterization of PEG Hydrogel Coatings

We engineered PEG-based coatings for neural electrodes (Fig. 1a). PEG has been used in implantable devices (58) and widely characterized as a non-fouling material with reduced protein adsorption and cell adhesion (59–61). Additionally, PEG-based coatings have been applied to neural electrodes with promising results *in vitro* including reduced cell adhesion and protein adsorption (23, 62). We generated coatings in which the PEG macromer was crosslinked via protease-degradable peptides that were substrates for the MMP-1 and MMP-2 (50, 63) as these proteases have been implicated as an important part of the inflammatory cascade in the brain (42, 46). Based on recent work by Patterson and Hubbell characterizing protease-degradable peptide sequences (63), we chose two protease-sensitive, crosslinking peptides: GCRDGDQGIAGFDRCG (GDQ) and GCRDVPMSMRGGDRCG (VPM). GDQ has very slow degradation kinetics (k_{cat} = 0.79 s^{-1} for MMP-1 and no observable degradation for MMP-2), whereas VPM has fast degradation kinetics (k_{cat} = 5.25 s^{-1} for MMP-1 and 4.82 s^{-1} for MMP-2). Importantly, these peptides contain cysteines at both ends of the molecule; the free thiol in these residues reacts rapidly with the maleimide group in the PEG macromers to produce a crosslinked hydrogel. These PEG-mal hydrogels and crosslinking peptides have been previously used successfully by our lab for other drug and cell delivery applications (54, 55, 64).

Silicon surfaces (electrode or Si wafer) were coated with the PEG-mal hydrogel coating. Fig. 1a shows a diagram of the predicted structure of the coating consisting of silane-PEG-mal, a protease degradable peptide crosslinker, and PEG-maleimide molecules. Fig. 1b presents XPS survey spectra for uncoated and 6-treatment PEG hydrogel-coated surfaces. As seen in the narrow band scans in Fig. 1c, clear shifts in the C1s peak demonstrate PEG-coated samples having a higher portion of C-C, H bonds as a result of coating deposition. The thickness of the coatings was analyzed by wet-cell ellipsometry. The thickness of the PEG coating increases with increasing treatment deposition, and a 6-treatment coating is approximately 30 nm thick (Fig. 1d, left), a reasonable measurement given the size of the coating components. Fig 1d (right) shows the difference in thickness between a 6-treatment coating of PEG and a 6-treatment coating with 2 treatments PEG and 4 treatments PEG +IL-1Ra, with the latter being thicker. The increased thickness for the PEG+IL-1Ra is not surprising given the incorporation of the anti-inflammatory protein (17 kDa, corresponding to a 3 nm diameter sphere (65)).

In Vitro Cell Adhesion

Silicon substrates were coated with one, two, or six treatments of PEG hydrogel using GDQ as the crosslinking peptide. Uncoated and PEG-coated surfaces were seeded with mixed glial cells (astrocytes + microglia) to evaluate cell adhesion to the coating. No differences in cell adhesion were observed between the PEG and PEG+IL-1Ra coatings. Greater than 90% of the cells on the surfaces were alive as determined by the Live/Dead stain. Image analysis

indicated that the PEG hydrogel reduces cell attachment and spreading compared to uncoated controls (Fig. 2a). The PEG coated samples had significantly reduced cell adhesion and spreading when analyzed by total area per attached cell (Fig. 2b, left), total number of attached cells (Fig. 2b, center), and total area covered by attached cells (Fig. 2b, right). The results indicate that the 6-treatment coating yielded the best reduction of cell adhesion and spreading. Additionally, the 2-treatment coating provided sufficient non-fouling behavior so that a 2-treatment non-degradable PEG coating can be used as a "base" coating for the additional 4-treatment PEG+IL-1Ra coating to yield a total of 6 treatments.

In Vitro Inflammatory Cytokine Release

Untreated and coated surfaces were tested to evaluate the release of cytokines, specifically IL-1β (Fig 3, left) and TNF-α (Fig 3, right), from mixed glial cells in response to stimulation with GM-CSF for 48 h. The levels of IL-1β were significantly higher on uncoated surfaces than those coated with PEG or PEG+IL-1Ra (detection limit = 5 pg/ml). TNF-α levels on the uncoated surface were significantly higher than the detection limit, whereas levels for the coated surfaces were below the detection limit (detection limit = 5 pg/ml). These results indicate that the PEG and PEG+IL-1Ra coatings reduce the release of inflammatory cytokines compared to uncoated surfaces. The lower cytokine levels are likely due to the lower number of adherent cells on these coated surfaces.

IL-1Ra Release from Hydrogel Coatings

Based on total release measurements, the hydrogel coating contains approximately 150 pg IL-1Ra in 0.3 μL of coating volume. Because human IL-1Ra has 4 cysteines that are not disulfide-linked (66) and are therefore available to react with the PEG-maleimide macromer, we expect the majority of IL-1Ra to be covalently tethered to the hydrogel network and only released following protease-dependent degradation of the hydrogel. In order to assess the stimulus-responsive release of IL-1Ra from the coating, we examined the release of IL-1Ra over time using an ELISA (Fig. 4). Samples were placed in conditioned media from cells stimulated with LPS (to induce secretion of MMP and other proteases to mimic the inflammatory environment associated with electrode implantation) or naïve media. Release data showed that samples incubated with LPS-stimulated cell culture media had an increasing release of IL-1Ra over time following a simple hyperbolic curve. Samples incubated in naive media had a basal level of release, probably due to gel swelling, showing that passive IL-1Ra release from the hydrogel is only 10% of the release for coatings incubated in conditioned media from LPS-treated glial cultures. This result demonstrates triggered release of IL-1Ra from the engineered coating.

Inflammatory Cell Recruitment, Astrogial Scarring, and BBB Breach around Implanted Electrodes

Electrode implantation and animal takedown were performed as described above. Immunostained histological sections for each group (n = 8 per group) were analyzed using the markers listed in Table 1, and intensity profiles were obtained via image analysis using the double exponential model described in the Methods section. This double exponential model captured the intensity profiles better than single exponential or KWW (5) models. For

the double exponential model, the R^2 values averaged 0.92 or greater for each IHC marker across all data sets.

Resident microglia were stained with OX42/CD11b (Fig. 5, Fig. S1). There were no significant differences among groups for $Intensity_1$, $Intensity_2$, and $Decay_{distal}$. However, the $Decay_{proximal}$ parameter was significantly higher for PEG+IL-1Ra compared to PEG coatings, showing that the intensity of resident microglial staining near the implant interface (0–100 μm) decays at a faster rate for PEG+IL-1Ra samples compared to other conditions.

Activated microglia were stained with ED1/CD68 (Fig. 6, Fig. S2) and astrocytes were stained with GFAP for glial fibrillary acidic protein (Fig. 7, Fig. S3). These stains showed no significant differences among groups for any parameters. These results indicate that neither the PEG coating nor the coating releasing IL-1Ra altered the distribution of these cell types in the vicinity of the implanted electrode.

Chondroitin sulfate antibody (CS56) was used to stain for glycosaminoglycans (GAG, Fig. 8, Fig. S4), which are a major extracellular matrix component of the astroglial scar. The $Decay_{distal}$ parameter was significantly lower for the PEG+IL-1Ra group compared to uncoated samples indicating that the amount of GAG staining decreases at a slow rate at distances far from the electrode surface (>100 μm).

Rat IgG was used as a marker for blood-brain barrier (BBB) breach (Fig. 9, Fig. S5), as this molecule permeates into brain tissue from comprised vasculature. The $Intensity_1$ parameter was significantly lower for PEG+IL-1Ra compared to uncoated surfaces, while the $Intensity_2$ parameter significantly lower for PEG+IL-1Ra compared to PEG surfaces. These differences indicate that the amount of IgG staining is lower around PEG+IL-1Ra coated electrodes, indicating a lower level of BBB breach. There were no differences among the decay parameters.

Neuronal Survival around Implanted Electrodes

To analyze neuronal survival, the number of cells positive for NeuN (neuronal nuclei) were counted at a distance of 0 – 500 μm from the implant insertion site (Fig. 10). Neuronal survival was elevated for both PEG and PEG+IL-1Ra coated electrodes compared to uncoated controls. Notably, closest to the electrode (0–50 μm bin), the number of NeuN+ cells in the PEG+IL-1Ra group was not significantly different from the uninjured contralateral control. In the 50–100 μm bin from the electrode surface, both PEG and PEG +IL-1Ra were not significantly different from the uninjured control. At distances 100+ μm from the interface, all three groups were not significantly different from the uninjured control. This data demonstrates increased neuronal survival around the electrode within the first 100 μm from the implant interface for the coated electrodes. This location is most critical for maintaining electrode functionality because the neurons closest to the electrode will provide the electrical signals that will be received by the electrode.

Gene Expression around Implanted Electrodes

Microfluidics-based quantitative RT-PCR was used to compare gene expression from the implant sites of brains (n = 7 per group) implanted with uncoated, PEG, or PEG+IL-1Ra

electrodes, as well as the contralateral uninjured control. Each graph shows the fold change of gene expression in each experimental group where each electrode-implanted sample is normalized to its matched uninjured control from the contralateral hemisphere. Gene expression analysis was conducted for the following gene targets: IL-1α, IL-1β, IL-1Ra, IL-6, IL-10, TNF-α, IFN-γ, MCP-1, MMP-2, MMP-3, MMP-9, MMP-13, NGF, GFAP, BDNF, and CNTF. The fold change differences for the genes are presented in Fig. 11, with the genes showing significant differences among groups outlined in green. Notably, many cytokines were markedly increased in the implantation site compared to the uninjured control including pro-inflammatory cytokines IL-1β, MCP-1, and IFN-γ as well as reparative cytokines such as IL-10 and IL-1Ra. Among the implanted electrodes, IL-6 was significantly higher in PEG+IL-1Ra compared to PEG alone while MMP-2 was significantly higher in PEG+IL-1Ra compared to uncoated samples. Additionally, CNTF was significantly higher in PEG+IL-1Ra electrodes than both uncoated and PEG samples.

Discussion

Chronically implanted neural electrodes cause local injury and an inflammatory response that leads to scar formation, neuronal death, and eventual electrode failure. To improve the tissue response to implanted electrodes, we engineered a polymer coating for neural electrodes that consists of a non-fouling, multi-layered PEG coating containing protease-degradable crosslinks and the anti-inflammatory agent IL-1Ra, which is released in response to proteases associated with the inflammatory response. XPS and wet-cell ellipsometry analyses demonstrated grafting of the coating on the surface as well as increasing coating thickness with increasing treatment deposition, respectively. To analyze cell adhesion to these coatings, surfaces were challenged with mixed glial cells in serum-containing media for 24 hours. PEG-coated surfaces with one, two, or six treatments were resistant to cell adhesion compared to uncoated surfaces as the total number of attached cells, average area per attached cell, and total cell attached area on each sample were all significantly lower than uncoated samples. In addition, cells plated on PEG or PEG+IL-1Ra coated surfaces had significantly lower levels of released pro-inflammatory cytokines IL-1β and TNF-α compared to uncoated surfaces, possibly due to the reduced cell attachment on these surfaces. These data indicate that the PEG-coated surfaces reduce glial cell adhesion and inflammatory cytokine release. This result is consistent with previous work with non-fouling/cell adhesion-resistant coatings (20). We also characterized the release of IL-1Ra from the engineered coating. Coatings incubated in conditioned media from LPS-treated cultures released significantly more IL-1Ra over time than the samples incubated in PBS, indicating the protease-dependent release of IL-1Ra from the degradable coating. We did not directly assess the bioactivity of the released IL-1Ra; however, our experience with this PEG hydrogel system has demonstrated excellent bioactivity for released protein therapeutics such as VEGF, BMP-2, and HGF (55, 64, 67). Additionally, the degradation products from these PEG hydrogels elicit no local or systemic toxicity and minimal inflammation and the degradation products are rapidly excreted via the urine (55). Collectively, these *in vitro* results demonstrate a promising cell adhesion-resistant and anti-inflammatory coating for evaluation in *in vivo* models.

Uncoated, PEG, and PEG+IL-1Ra coated electrodes were implanted in the brain of rats for 4 weeks to evaluate the *in vivo* response of the brain to implanted electrodes. Samples were collected, cryosectioned, and stained for markers to analyze cell responses to the implanted electrode as well as blood brain barrier breach. Staining for resident microglia (OX42/CD11b) showed no differences in $Intensity_1$, $Intensity_2$, and $Decay_{distal}$ parameters among groups. However, the $Decay_{proximal}$ parameter was significantly higher for PEG+IL-1Ra compared to PEG coatings, indicating that the intensity of resident microglial staining near the implant interface (0–100 μm) decays at a faster rate for PEG+IL-1Ra samples. This reduction in the OX42 $Decay_{proximal}$ parameter suggests that the IL-1Ra attenuates microglial recruitment to the electrode-tissue interface.

Staining for activated microglia (ED1/CD11b) and astrocytes (GFAP) revealed no significant differences for any of the parameters among the groups. We hypothesized that the anti-inflammatory factor incorporated into the PEG-coating would reduce the inflammatory response in the surrounding tissue. However, persistence of activated microglia around the implant for all experimental groups indicates that neither the PEG coating nor the incorporated IL-1Ra prevent microglial activation and astrocyte recruitment. Since microglial activation is an important part of the inflammatory cascade, it is apparent that inflammation persists in the tissue. Additionally, we expected that the non-fouling PEG surface would reduce astrocyte recruitment and subsequent scar formation; however, this did not occur in the rat model. Staining for chondroitin sulfate (CS56) indicates the presence of glycosaminoglycans, an important component of the astroglial scar. The $Decay_{distal}$ parameter was significantly higher for uncoated samples compared to PEG+IL-1Ra for CS56, indicating a faster decrease of CS56 staining at areas >100 μm from the injury site. This indicates that there is less glycosaminoglycan staining around uncoated electrodes at distances far from the implant site.

Although no differences were observed among groups for astrocyte and microglial recruitment, significant differences were observed in IgG staining around the electrode among the coating conditions. IgG staining serves a surrogate for BBB breach (11). The lower IgG $Intenisty_1$ and $Intensity_2$ parameters for PEG+IL-1Ra compared to uncoated and PEG coated electrodes, respectively, indicates that the amount of BBB breach around the PEG+IL-1Ra coated electrodes is significantly reduced compared to the uncoated and PEG electrodes. This is an important finding because the persistence of the electrode in the tissue and the subsequent continued BBB breach are correlated with persistence of inflammation in the brain (11), and reducing the effect of BBB breach may reduce deleterious inflammatory responses in the long term. Moreover, Bellamkonda's group has demonstrated a specific correlation between reduced BBB breach and improved electrode functionality (5, 11). At this point, it is not known if the reduction in BBB breach is due to a reduction of the initial inflammatory response, faster healing response over time, or a combination of the two in the presence of the IL-1Ra, but this would be an interesting aspect to explore in future studies. Whether the PEG coatings and IL-1Ra release improve electrode function will be the subject of future studies.

Finally, NeuN staining for neuronal nuclei showed significant differences in neuronal survival among the three groups. We observed increased neuronal survival for the PEG

+IL-1Ra electrodes within 50 μm of the electrode surface, and the density of neuronal nuclei were equivalent to that of the injured control. Additionally, increased neuronal survival was detected at intermediate distances (50–100 μm) from the electrode surface for PEG- and PEG+IL-1Ra-coated electrodes compared to uncoated controls. This is an important finding because neurons are necessary for electrode functionality. If the neurons surrounding the implant do not survive after electrode insertion, then the electrode cannot receive any electrical signals from the surrounding tissue, rendering the device useless. Increasing neuronal survival is essential to maintaining long-term electrode function. The ideal response of the brain would result in no neuronal death upon implantation of a neural electrode. However, improvement within the first 100 μm is a promising finding as electrodes can record neuronal activity to a radius of ~100 microns or more from the electrode surface (68).

Analysis of gene expression in the brain around the electrode implantation site yielded important insights into the tissue responses to implanted electrodes. Of the 16 genes that were analyzed, only three had significant differences among groups. IL-6 gene expression was significantly higher in the PEG+IL-1Ra group compared to the PEG group. While IL-6 is traditionally considered a pro-inflammatory cytokine (69), there is evidence that it plays a role in activation of downstream cell-survival and anti-apoptotic factors (70). The up-regulation of MMP-2 in the PEG+IL-1Ra group compared to the uncoated group is an interesting finding. MMP-2 is found in activated astrocytes (71), which is consistent with the presence of recruited astrocytes around the implanted electrode. The increase in MMP-2 for the PEG+IL-1Ra group is also contradictory to some extent, as MMP-2 is implicated in promoting BBB breach (71), but the IgG staining intensity was significantly lower for PEG +IL-1Ra samples. It is possible that the release of MMP-2 is occurring in response to down-regulation of other inflammatory cytokines, as there are many redundant signaling pathways. Alternatively, MMP-2 up-regulation may reflect the activation of tissue repair mechanisms. Regardless, the up-regulation of MMP gene expression in the injury site validates the use of this protease-degradable coating as the MMPs will cause desired degradation of the coating and release of the anti-inflammatory therapeutic.

Gene expression of neural-specific markers showed significantly higher expression for cilliary neurotrophic factor (CNTF) in PEG+IL-1Ra coated electrodes compared to PEG and uncoated groups. CNTF is important for neuronal survival and neurite outgrowth (72). Interestingly, IL-1β is required for the production of CNTF (73), indicating that inflammatory cytokines can play a role in both pro-inflammatory activation as well as anti-inflammatory cytokine activation downstream. The lack of differences in NGF and BDNF were unexpected given the increased neuronal survival found in the PEG+IL-1Ra group, however this may also indicate that other factors such as CNTF or others not investigated here may play a more significant role in neuronal survival. Overall, the results from the gene expression studies are generally consistent with the findings from the immunostaining analyses, showing persistence of inflammation and increased expression of a neuronal survival gene. These results also identify possible targets for future research into inflammation and neuronal survival in the brain.

One important observation is the need for better *in vitro* evaluation techniques. The 2D cell culture system is a good starting point, but further evaluation with more complex *in vitro* systems is necessary to determine if a particular coating can perform well *in vivo*. While both 2D and 3D culture systems have been used for *in vitro* evaluation, they do not recapitulate the host response to electrode surfaces since these *in vitro* models do not include vasculature, BBB breach, and subsequent inflammatory responses. The complexity of the vasculature and associated BBB breach is an especially important aspect to address, although it is difficult to recapitulate in an *in vitro* model. Research towards developing a more complete *in vitro* system of brain tissue may provide suitable platform for electrode evaluation prior to *in vivo* analyses.

Many strategies have been explored to improve tissue response to implanted neural electrodes through design modifications, surface coatings, and incorporation of anti-inflammatory factors. None of the attempted coatings to date have solved all problems involved with implanted neural electrodes due to the complicated nature of the injury which includes inflammation, cell recruitment, scar formation, and neuronal cell death. Although we observed significant reductions in glial cell adhesion and inflammatory cytokine release *in vitro*, no major differences were observed in the recruitment and activation of inflammatory cells and scar formation among implanted electrodes. These results suggest that reduction of cell adhesion alone is insufficient for improving the cell recruitment and subsequent scar formation. In addition, *in vitro* culture systems do not recapitulate all aspects of the complex inflammatory cascade and vascular injury associated with electrode implantation. Nevertheless, the significant improvement in neuronal survival for the coated and IL-1Ra-releasing coatings is a promising finding as neuronal survival is central to maintaining electrode functionality. Overall, more work needs to be done to determine an effective strategy for maintaining neural electrode functionality in the long term.

Conclusions

The coating developed in this study consists of a PEG coated surface cross-linked with protease degradable peptide sequences that release IL-1Ra in response to inflammatory stimuli. This coating significantly reduced *in vitro* glial cell attachment and inflammatory cytokine release, and demonstrated IL-1Ra release from coated samples. Subsequent *in vivo* studies indicated only minor improvements in inflammatory cell markers. However, IgG staining, a surrogate for blood-brain barrier breach, was reduced for PEG+IL-1Ra coatings compared to uncoated electrodes. Importantly, neuronal survival was significantly higher for coated electrodes, with the best improvement observed for the PEG+IL-1Ra group. Additionally, results from the gene expression analysis study indicate potential targets for future therapies which may be useful in producing better modifications to improve the tissue response to implanted electrodes. This PEG coating with on-demand release of IL-1Ra shows promise for enhancement of tissue responses at the brain-implant interface.

Supplementary Material

Refer to Web version on PubMed Central for supplementary material.

Acknowledgements

This work was supported by National Institutes of Health Grants: F31NS073358 (SMG) and T32EB006343-01A2 (RVB); GAANN Fellowship for Drug Design, Development, and Delivery (US Department of Education P200A090099); Georgia Tech/Emory Center for the Engineering of Living Tissues and the Atlanta Clinical and Translational Science Institute under PHS Grant UL RR025008 from the Clinical and Translational Science Award Program. We acknowledge the valuable insight through discussions with Drs. Garret Stanley and Robert Gross. XPS analysis was performed by the National ESCA and Surface Analysis Center for Biomedical Problems (NESAC/BIO, NIH EB-002027).

References

1. Schwartz AB, Cui XT, Weber DJ, Moran DW. Brain-controlled interfaces: movement restoration with neural prosthetics. Neuron. 2006; 52(1):205–220. [PubMed: 17015237]
2. Lebedev MA, Nicolelis MA. Brain-machine interfaces: past, present and future. Trends Neurosci. 2006; 29(9):536–546. [PubMed: 16859758]
3. Birbaumer N, Cohen LG. Brain-computer interfaces: communication and restoration of movement in paralysis. The Journal of physiology. 2007; 579(Pt 3):621–636. [PubMed: 17234696]
4. Donoghue JP. Connecting cortex to machines: recent advances in brain interfaces. Nat Neurosci. 2002; (5 Suppl):1085–1088. [PubMed: 12403992]
5. Karumbaiah L, Saxena T, Carlson D, Patil K, Patkar R, Gaupp EA, et al. Relationship between intracortical electrode design and chronic recording function. Biomaterials. 2013; 34(33):8061–8074. [PubMed: 23891081]
6. Szarowski DH, Andersen MD, Retterer S, Spence AJ, Isaacson M, Craighead HG, et al. Brain responses to micro-machined silicon devices. Brain Res. 2003; 983(1–2):23–35. [PubMed: 12914963]
7. Biran R, Martin DC, Tresco PA. Neuronal cell loss accompanies the brain tissue response to chronically implanted silicon microelectrode arrays. Exp Neurol. 2005; 195(1):115–126. [PubMed: 16045910]
8. Polikov VS, Tresco PA, Reichert WM. Response of brain tissue to chronically implanted neural electrodes. J Neurosci Methods. 2005; 148(1):1–18. [PubMed: 16198003]
9. Fattahi P, Yang G, Kim G, Abidian MR. A Review of Organic and Inorganic Biomaterials for Neural Interfaces. Adv Mater. 2014
10. McConnell GC, Rees HD, Levey AI, Gutekunst CA, Gross RE, Bellamkonda RV. Implanted neural electrodes cause chronic, local inflammation that is correlated with local neurodegeneration. J Neural Eng. 2009; 6(5):056003. [PubMed: 19700815]
11. Saxena T, Karumbaiah L, Gaupp EA, Patkar R, Patil K, Betancur M, et al. The impact of chronic blood-brain barrier breach on intracortical electrode function. Biomaterials. 2013; 34(20):4703–4713. [PubMed: 23562053]
12. Potter KA, Buck AC, Self WK, Capadona JR. Stab injury and device implantation within the brain results in inversely multiphasic neuroinflammatory and neurodegenerative responses. J Neural Eng. 2012; 9(4):046020. [PubMed: 22832283]
13. Ludwig KA, Uram JD, Yang J, Martin DC, Kipke DR. Chronic neural recordings using silicon microelectrode arrays electrochemically deposited with a poly(3,4-ethylenedioxythiophene) (PEDOT) film. J Neural Eng. 2006; 3(1):59–70. [PubMed: 16510943]
14. Pierce AL, Sommakia S, Rickus JL, Otto KJ. Thin-film silica sol-gel coatings for neural microelectrodes. J Neurosci Methods. 2009; 180(1):106–110. [PubMed: 19427536]
15. Cui X, Lee VA, Raphael Y, Wiler JA, Hetke JF, Anderson DJ, et al. Surface modification of neural recording electrodes with conducting polymer/biomolecule blends. J Biomed Mater Res. 2001; 56(2):261–272. [PubMed: 11340598]
16. Cui X, Martin DC. Electrochemical deposition and characterization of poly(3,4-ethylenedioxythiophene) on neural microelectrode arrays. Sensors and Actuators B: Chemical. 2003; 89(1–2):92–102.
17. Cui X, Wiler J, Dzaman M, Altschuler RA, Martin DC. In vivo studies of polypyrrole/peptide coated neural probes. Biomaterials. 2003; 24(5):777–787. [PubMed: 12485796]

18. Abidian MR, Corey JM, Kipke DR, Martin DC. Conducting-polymer nanotubes improve electrical properties, mechanical adhesion, neural attachment, and neurite outgrowth of neural electrodes. Small. 2010; 6(3):421–429. [PubMed: 20077424]
19. Di L, Wang LP, Lu YN, He L, Lin ZX, Wu KJ, et al. Protein adsorption and peroxidation of rat retinas under stimulation of a neural probe coated with polyaniline. Acta biomaterialia. 2011; 7(10):3738–3745. [PubMed: 21704201]
20. Leung BK, Biran R, Underwood CJ, Tresco PA. Characterization of microglial attachment and cytokine release on biomaterials of differing surface chemistry. Biomaterials. 2008; 29(23):3289–3297. [PubMed: 18485471]
21. Gutowski SM, Templeman KL, South AB, Gaulding JC, Shoemaker JT, LaPlaca MC, et al. Host response to microgel coatings on neural electrodes implanted in the brain. J Biomed Mater Res A. 2014; 102(5):1486–1499. [PubMed: 23666919]
22. Lu Y, Wang D, Li T, Zhao X, Cao Y, Yang H, et al. Poly(vinyl alcohol)/poly(acrylic acid) hydrogel coatings for improving electrode-neural tissue interface. Biomaterials. 2009; 30(25): 4143–4151. [PubMed: 19467702]
23. Rao L, Zhou H, Li T, Li C, Duan YY. Polyethylene glycol-containing polyurethane hydrogel coatings for improving the biocompatibility of neural electrodes. Acta biomaterialia. 2012; 8(6): 2233–2242. [PubMed: 22406507]
24. Bezuidenhout D, Oosthuysen A, Davies N, Ahrenstedt L, Dobner S, Roberts P, et al. Covalent incorporation and controlled release of active dexamethasone from injectable polyethylene glycol hydrogels. J Biomed Mater Res A. 2013; 101(5):1311–1318. [PubMed: 23065782]
25. Zhong, Y.; McConnell, GC.; Ross, JD.; DeWeerth, SP.; Bellamkonda, RV. A Novel Dexamethasone-releasing, Antiinflammatory Coating for Neural Implants; Proceedings of the 2 International IEEE EMBS. 2005 (2nd International IEEE EMBS Conference on Neural Engineering); p. 522
26. Zhong Y, Bellamkonda RV. Dexamethasone-coated neural probes elicit attenuated inflammatory response and neuronal loss compared to uncoated neural probes. Brain Res. 2007; 1148:15–27. [PubMed: 17376408]
27. Kim DH, Martin DC. Sustained release of dexamethasone from hydrophilic matrices using PLGA nanoparticles for neural drug delivery. Biomaterials. 2006; 27(15):3031–3037. [PubMed: 16443270]
28. Mercanzini A, Reddy ST, Velluto D, Colin P, Maillard A, Bensadoun JC, et al. Controlled release nanoparticle-embedded coatings reduce the tissue reaction to neuroprostheses. J Control Release. 2010; 145(3):196–202. [PubMed: 20447428]
29. Shain W, Spataro L, Dilgen J, Haverstick K, Retterer S, Isaacson M, et al. Controlling cellular reactive responses around neural prosthetic devices using peripheral and local intervention strategies. Ieee T Neur Sys Reh. 2003; 11(2):186–188.
30. Spataro L, Dilgen J, Retterer S, Spence AJ, Isaacson M, Turner JN, et al. Dexamethasone treatment reduces astroglia responses to inserted neuroprosthetic devices in rat neocortex. Exp Neurol. 2005; 194(2):289–300. [PubMed: 16022859]
31. Zhong Y, Bellamkonda RV. Controlled release of anti-inflammatory agent alpha-MSH from neural implants. J Control Release. 2005; 106(3):309–318. [PubMed: 15978692]
32. Klaver CL, Caplan MR. Bioactive surface for neural electrodes: decreasing astrocyte proliferation via transforming growth factor-beta1. J Biomed Mater Res A. 2007; 81(4):1011–1016. [PubMed: 17265435]
33. Abidian MR, Martin, David C. Multifunctional Nanobiomaterials for Neural Interfaces. Advanced Functional Materials. 2009; 19:573–585.
34. Wadhwa R, Lagenaur CF, Cui XT. Electrochemically controlled release of dexamethasone from conducting polymer polypyrrole coated electrode. J Control Release. 2006; 110(3):531–541. [PubMed: 16360955]
35. Potter KA, Jorfi M, Householder KT, Foster EJ, Weder C, Capadona JR. Curcumin-releasing mechanically adaptive intracortical implants improve the proximal neuronal density and blood-brain barrier stability. Acta biomaterialia. 2014; 10(5):2209–2222. [PubMed: 24468582]

36. Arend WP. The balance between IL-1 and IL-1Ra in disease. Cytokine & growth factor reviews. 2002; 13(4–5):323–340. [PubMed: 12220547]
37. Arend WP, Malyak M, Guthridge CJ, Gabay C. Interleukin-1 receptor antagonist: role in biology. Annual review of immunology. 1998; 16:27–55.
38. Pinteaux E, Rothwell NJ, Boutin H. Neuroprotective actions of endogenous interleukin-1 receptor antagonist (IL-1ra) are mediated by glia. Glia. 2006; 53(5):551–556. [PubMed: 16374779]
39. Taub AH, Hogri R, Magal A, Mintz M, Shacham-Diamand Y. Bioactive anti-inflammatory coating for chronic neural electrodes. J Biomed Mater Res A. 2012; 100(7):1854–1858. [PubMed: 22488754]
40. Malemud CJ. Matrix metalloproteinases (MMPs) in health and disease: an overview. Frontiers in bioscience : a journal and virtual library. 2006; 11:1696–1701. [PubMed: 16368548]
41. Manicone AM, McGuire JK. Matrix metalloproteinases as modulators of inflammation. Seminars in cell & developmental biology. 2008; 19(1):34–41. [PubMed: 17707664]
42. Rosenberg GA. Matrix metalloproteinases and their multiple roles in neurodegenerative diseases. Lancet neurology. 2009; 8(2):205–216.
43. Ferguson TA, Muir D. MMP-2 and MMP-9 increase the neurite-promoting potential of schwann cell basal laminae and are upregulated in degenerated nerve. Molecular and cellular neurosciences. 2000; 16(2):157–167. [PubMed: 10924258]
44. Goussev S, Hsu JY, Lin Y, Tjoa T, Maida N, Werb Z, et al. Differential temporal expression of matrix metalloproteinases after spinal cord injury: relationship to revascularization and wound healing. Journal of neurosurgery. 2003; 99(2 Suppl):188–197. [PubMed: 12956462]
45. Gursoy-Ozdemir Y, Qiu J, Matsuoka N, Bolay H, Bermpohl D, Jin H, et al. Cortical spreading depression activates and upregulates MMP-9. The Journal of clinical investigation. 2004; 113(10): 1447–1455. [PubMed: 15146242]
46. Rosenberg GA. Matrix metalloproteinases in brain injury. J Neurotrauma. 1995; 12(5):833–842. [PubMed: 8594211]
47. Lo EH, Wang X, Cuzner ML. Extracellular proteolysis in brain injury and inflammation: role for plasminogen activators and matrix metalloproteinases. J Neurosci Res. 2002; 69(1):1–9. [PubMed: 12111810]
48. Karumbaiah L, Norman SE, Rajan NB, Anand S, Saxena T, Betancur M, et al. The upregulation of specific interleukin (IL) receptor antagonists and paradoxical enhancement of neuronal apoptosis due to electrode induced strain and brain micromotion. Biomaterials. 2012; 33(26):5983–5996. [PubMed: 22681976]
49. Anderson SB, Lin CC, Kuntzler DV, Anseth KS. The performance of human mesenchymal stem cells encapsulated in cell-degradable polymer-peptide hydrogels. Biomaterials. 2011; 32(14): 3564–3574. [PubMed: 21334063]
50. Patterson J, Hubbell JA. Enhanced proteolytic degradation of molecularly engineered PEG hydrogels in response to MMP-1 and MMP-2. Biomaterials. 2010; 31(30):7836–7845. [PubMed: 20667588]
51. Bott K, Upton Z, Schrobback K, Ehrbar M, Hubbell JA, Lutolf MP, et al. The effect of matrix characteristics on fibroblast proliferation in 3D gels. Biomaterials. 2010; 31(32):8454–8464. [PubMed: 20684983]
52. Bracher M, Bezuidenhout D, Lutolf MP, Franz T, Sun M, Zilla P, et al. Cell specific ingrowth hydrogels. Biomaterials. 2013; 34(28):6797–6803. [PubMed: 23777918]
53. Tauro JR, Gemeinhart RA. Matrix metalloprotease triggered delivery of cancer chemotherapeutics from hydrogel matrixes. Bioconjug Chem. 2005; 16(5):1133–1139. [PubMed: 16173790]
54. Phelps EA, Enemchukwu NO, Fiore VF, Sy JC, Murthy N, Sulchek TA, et al. Maleimide cross-linked bioactive PEG hydrogel exhibits improved reaction kinetics and cross-linking for cell encapsulation and in situ delivery. Adv Mater. 2012; 24(1):64–70. 2. [PubMed: 22174081]
55. Phelps EA, Headen DM, Taylor WR, Thule PM, Garcia AJ. Vasculogenic bio-synthetic hydrogel for enhancement of pancreatic islet engraftment and function in type 1 diabetes. Biomaterials. 2013; 34(19):4602–4611. [PubMed: 23541111]
56. Zisch AH, Lutolf MP, Ehrbar M, Raeber GP, Rizzi SC, Davies N, et al. Cell-demanded release of VEGF from synthetic, biointeractive cell ingrowth matrices for vascularized tissue growth.

FASEB journal : official publication of the Federation of American Societies for Experimental Biology. 2003; 17(15):2260–2262. [PubMed: 14563693]

57. Frampton JP, Hynd MR, Shuler ML, Shain W. Effects of glial cells on electrode impedance recorded from neuralprosthetic devices in vitro. Annals of biomedical engineering. 2010; 38(3): 1031–1047. [PubMed: 20336824]
58. Hoffman AS. Non-fouling surface technologies. J Biomater Sci Polym Ed. 1999; 10(10):1011–1014. [PubMed: 10591129]
59. Harbers GM, Emoto K, Greef C, Metzger SW, Woodward HN, Mascali JJ, et al. A functionalized poly(ethylene glycol)-based bioassay surface chemistry that facilitates bio-immobilization and inhibits non-specific protein, bacterial, and mammalian cell adhesion. Chemistry of materials : a publication of the American Chemical Society. 2007; 19(18):4405–4414. [PubMed: 18815622]
60. Zhang F, Kang ET, Neoh KG, Wang P, Tan KL. Surface modification of stainless steel by grafting of poly(ethylene glycol) for reduction in protein adsorption. Biomaterials. 2001; 22(12):1541–1548. [PubMed: 11374453]
61. Zhang M, Desai T, Ferrari M. Proteins and cells on PEG immobilized silicon surfaces. Biomaterials. 1998; 19(10):953–960. [PubMed: 9690837]
62. Sharma S, Johnson RW, Desai TA. Evaluation of the stability of nonfouling ultrathin poly(ethylene glycol) films for silicon-based microdevices. Langmuir. 2004; 20(2):348–356. [PubMed: 15743077]
63. Patterson J, Hubbell JA. SPARC-derived protease substrates to enhance the plasmin sensitivity of molecularly engineered PEG hydrogels. Biomaterials. 2011; 32(5):1301–1310. [PubMed: 21040970]
64. Shekaran A, Garcia JR, Clark AY, Kavanaugh TE, Lin AS, Guldberg RE, et al. Bone regeneration using an alpha 2 beta 1 integrin-specific hydrogel as a BMP-2 delivery vehicle. Biomaterials. 2014; 35(21):5453–5461. [PubMed: 24726536]
65. Erickson HP. Size and shape of protein molecules at the nanometer level determined by sedimentation, gel filtration, and electron microscopy. Biological procedures online. 2009; 11:32–51. [PubMed: 19495910]
66. Steinkasserer A, Solari R, Mott HR, Aplin RT, Robinson CC, Willis AC, et al. Human interleukin-1 receptor antagonist. High yield expression in E. coli and examination of cysteine residues. FEBS Lett. 1992; 310(1):63–65. [PubMed: 1388125]
67. Salimath AS, Phelps EA, Boopathy AV, Che PL, Brown M, Garcia AJ, et al. Dual delivery of hepatocyte and vascular endothelial growth factors via a protease-degradable hydrogel improves cardiac function in rats. PLoS One. 2012; 7(11):e50980. [PubMed: 23226440]
68. Buzsaki G. Large-scale recording of neuronal ensembles. Nat Neurosci. 2004; 7(5):446–451. [PubMed: 15114356]
69. Steinman L. Inflammatory cytokines at the summits of pathological signal cascades in brain diseases. Science signaling. 2013; 6(258):e3.
70. Smith JA, Das A, Ray SK, Banik NL. Role of pro-inflammatory cytokines released from microglia in neurodegenerative diseases. Brain Res Bull. 2012; 87(1):10–20. [PubMed: 22024597]
71. Rosenberg GA, Cunningham LA, Wallace J, Alexander S, Estrada EY, Grossetete M, et al. Immunohistochemistry of matrix metalloproteinases in reperfusion injury to rat brain: activation of MMP-9 linked to stromelysin-1 and microglia in cell cultures. Brain Res. 2001; 893(1–2):104–112. [PubMed: 11222998]
72. Ip NY, Li YP, van de Stadt I, Panayotatos N, Alderson RF, Lindsay RM. Ciliary neurotrophic factor enhances neuronal survival in embryonic rat hippocampal cultures. The Journal of neuroscience : the official journal of the Society for Neuroscience. 1991; 11(10):3124–3134. [PubMed: 1941077]
73. Herx LM, Rivest S, Yong VW. Central nervous system-initiated inflammation and neurotrophism in trauma: IL-1 beta is required for the production of ciliary neurotrophic factor. J Immunol. 2000; 165(4):2232–2239. [PubMed: 10925311]

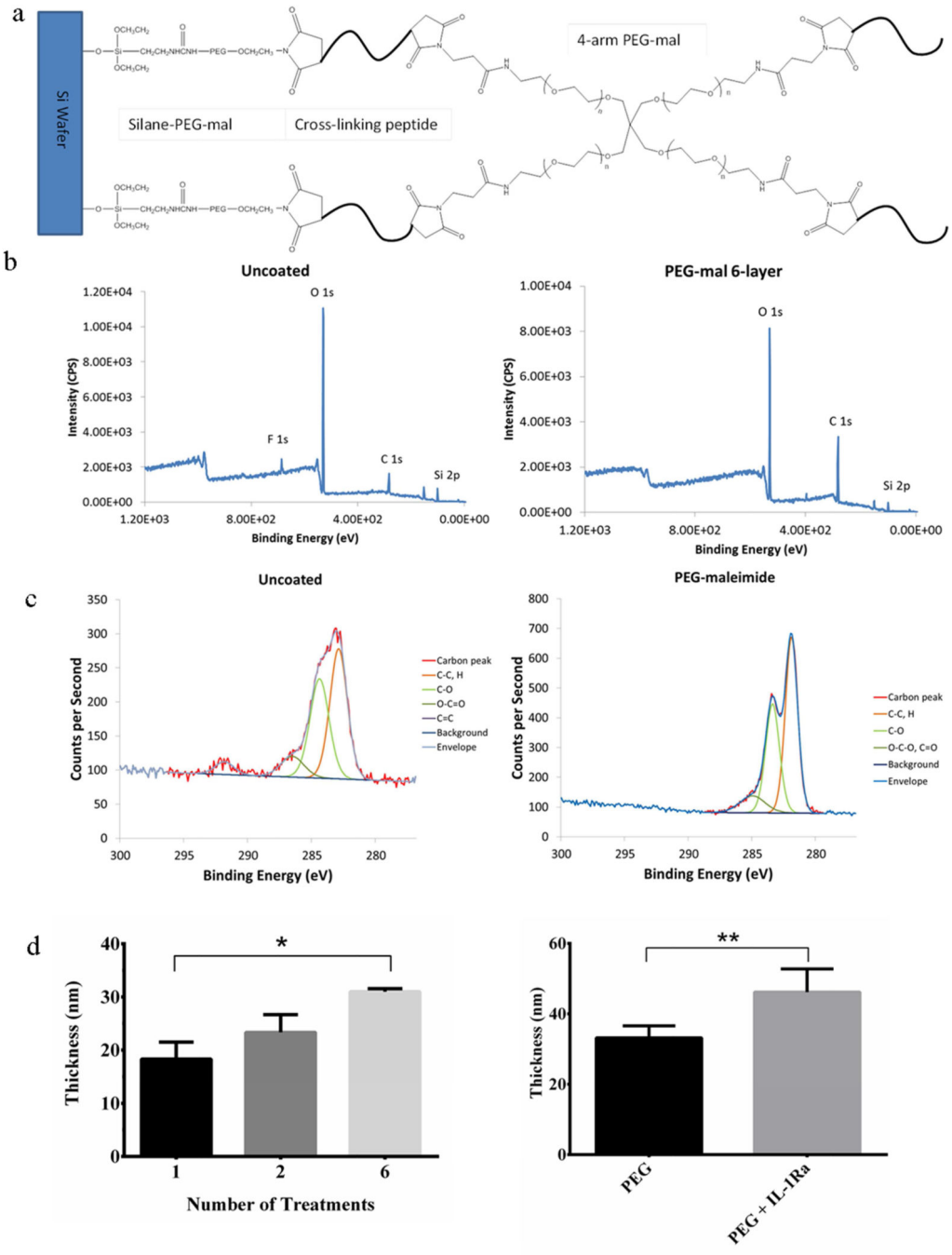

Figure 1.

PEG coatings applied to the surface of electrodes. (a) Schematic of PEG hydrogel coating applied to the surface of the silicon substrate. (b) XPS spectra of uncoated (left) and PEG coated (right) electrodes. (c) Detailed carbon shifts of the uncoated (left) and PEG-coated (right) surfaces. (d) PEG coating thickness. Thickness of the coating increases with increasing number of treatments applied to the surface (left). Incorporating IL-1Ra yields a thicker coating than with the PEG alone (right). * = $p<0.05$, ** = $p<0.01$.

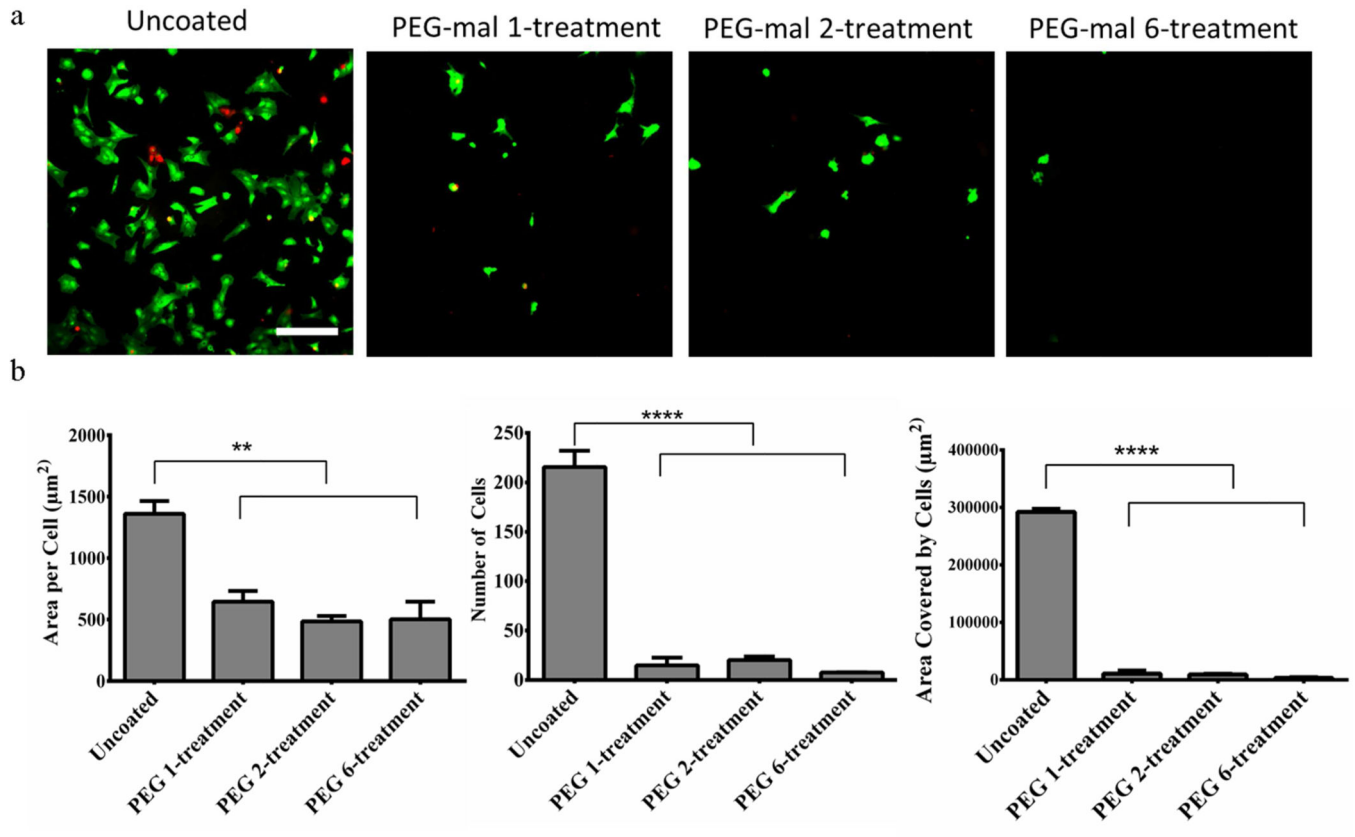

Figure 2.

Cell adhesion for various PEG treatments. Live/Dead stain of cells adhering to uncoated and PEG-coated surfaces with 1, 2, or 6 treatment cycles (top). Scale bar = 250 μm. Area per attached cell (bottom, left), total number of cells adhered (bottom, middle), and total area covered by adhered cells on the surface (bottom, right) is significantly lower on PEG coated surfaces than uncoated surfaces. ** = $p<0.01$, **** = $p<0.0001$.

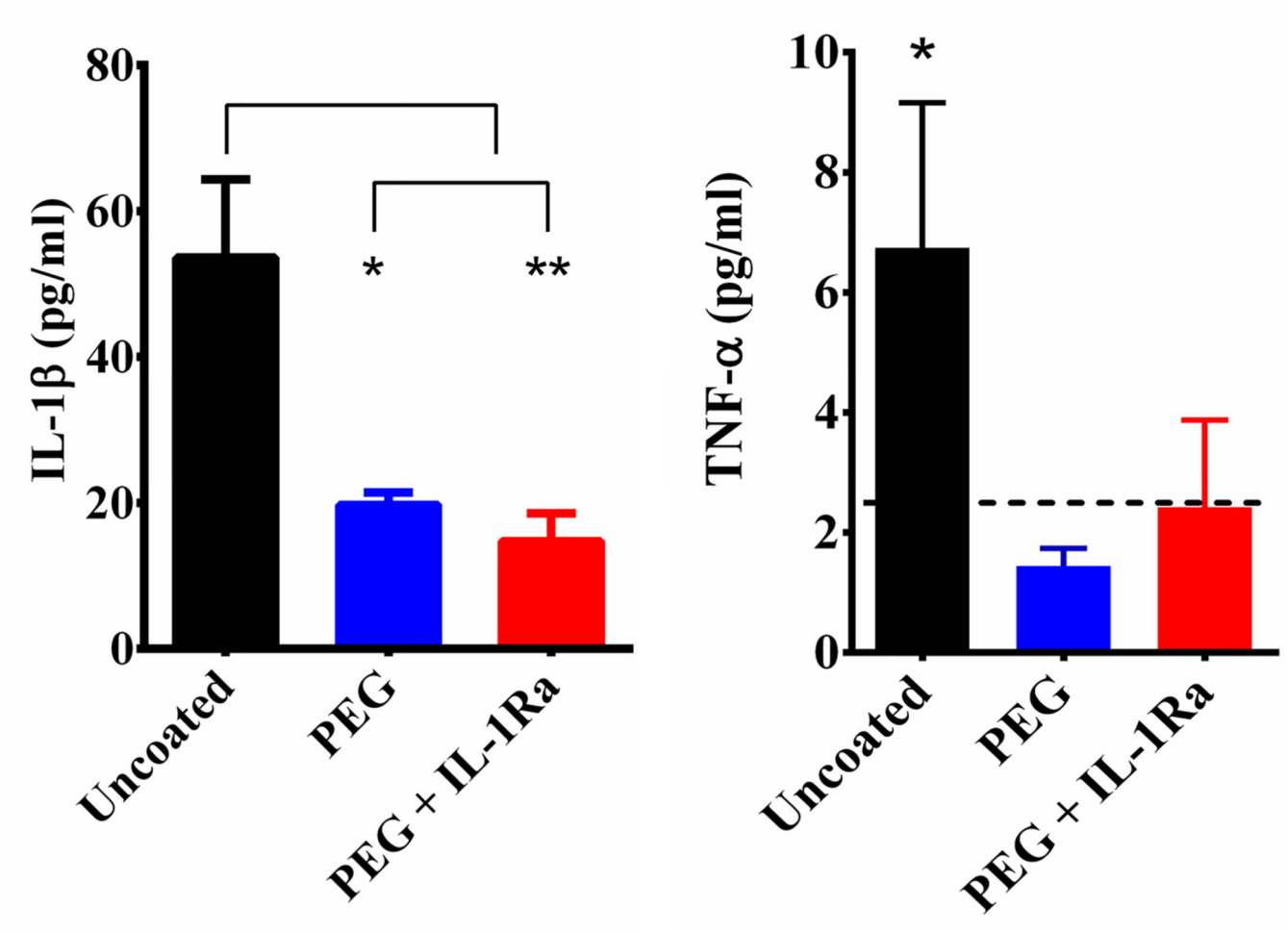

Figure 3.

Cytokine release for cells cultured on uncoated, PEG-, and PEG+IL-1Ra-coated surfaces in response to GM-CSF stimulation. IL-1β was significantly higher on uncoated surfaces compared to coated surfaces (left). TNF-α was significantly higher than background for the uncoated surface, and levels on coated surfaces were below detection limit of the assay (dashed line) (right). * = $p<0.05$, ** = $p<0.01$.

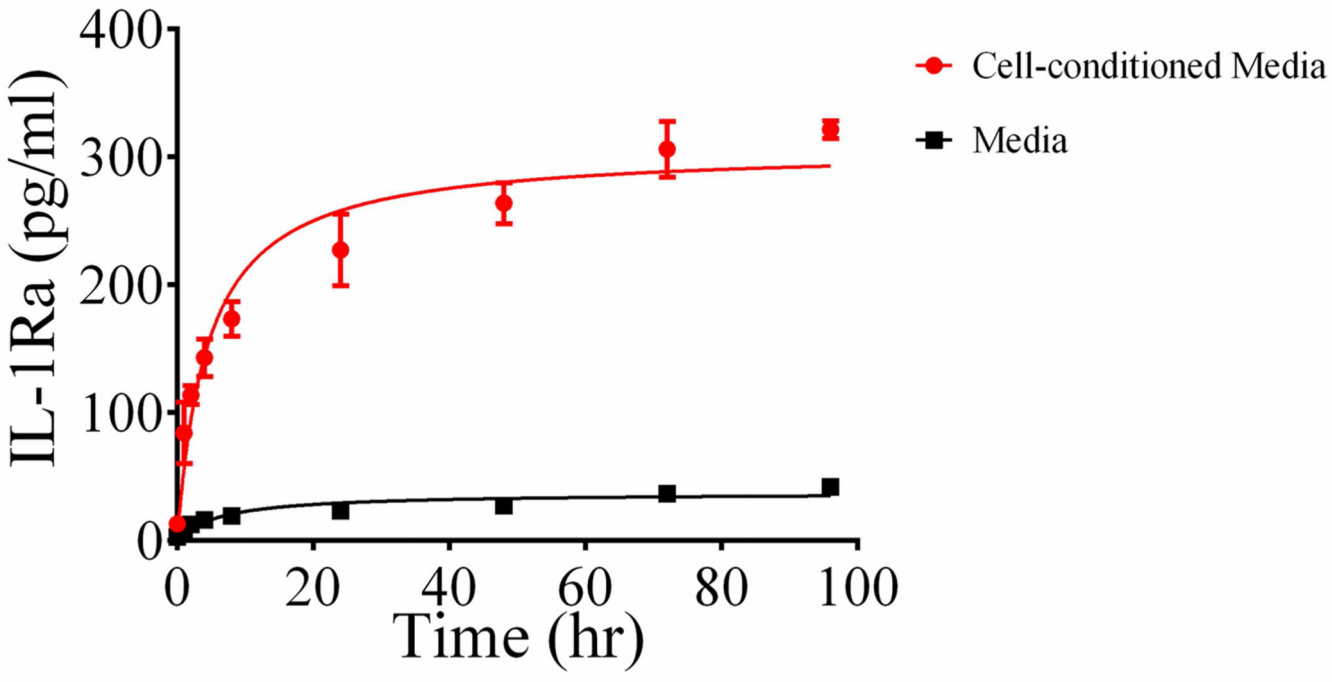

Figure 4.

IL-1Ra release curve shows that IL-1Ra release is higher with LPS-stimulated cell media compared to media alone. Shown are individual points (mean ± SEM) and hyperbolic fits.

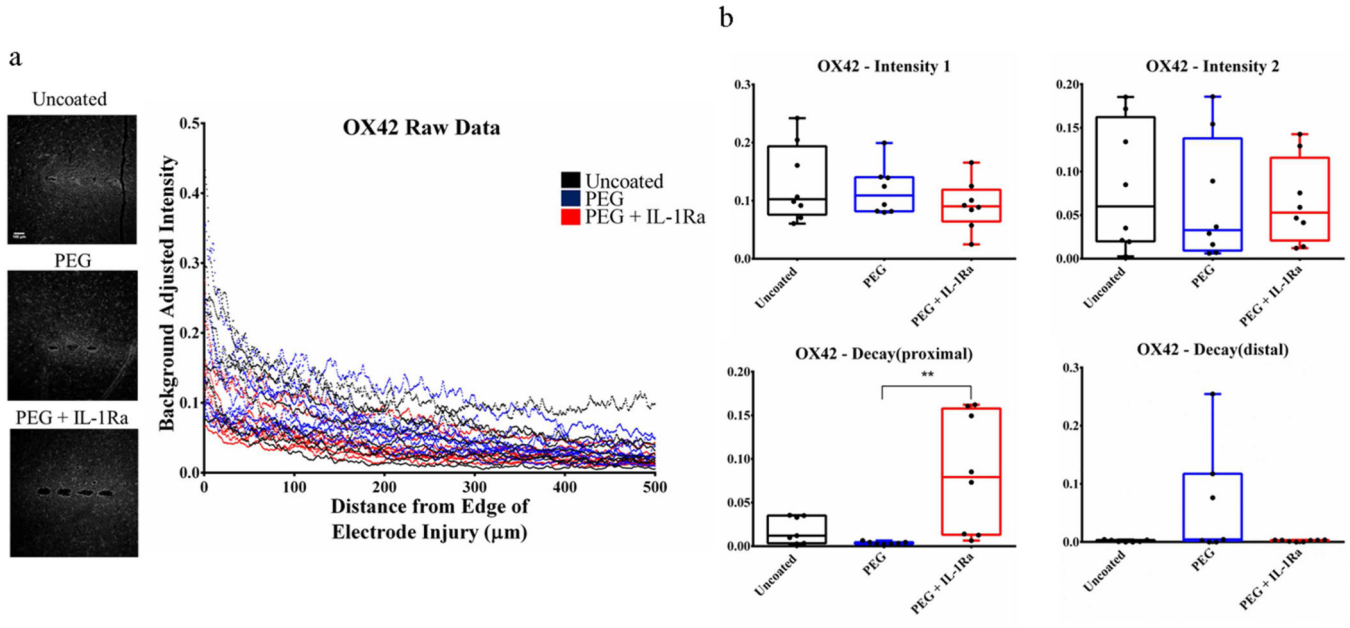

Figure 5.

Immunofluorescence analysis for resident microglia (OX42). (a) Immunofluorescence images (left) and corresponding intensity profile (right) for uncoated, PEG, and PEG +IL-1Ra (n=8 per group). (b) Parameter plots indicate differences in each parameter of Equation 1 for each experimental group. The $Decay_{proximal}$ parameter is significantly higher for PEG+IL-1Ra compared to PEG alone. The box plots indicate minimum, 25th percentile, median, 75th percentile, and maximum, with individual points shown for each sample. ** = $p<0.01$.

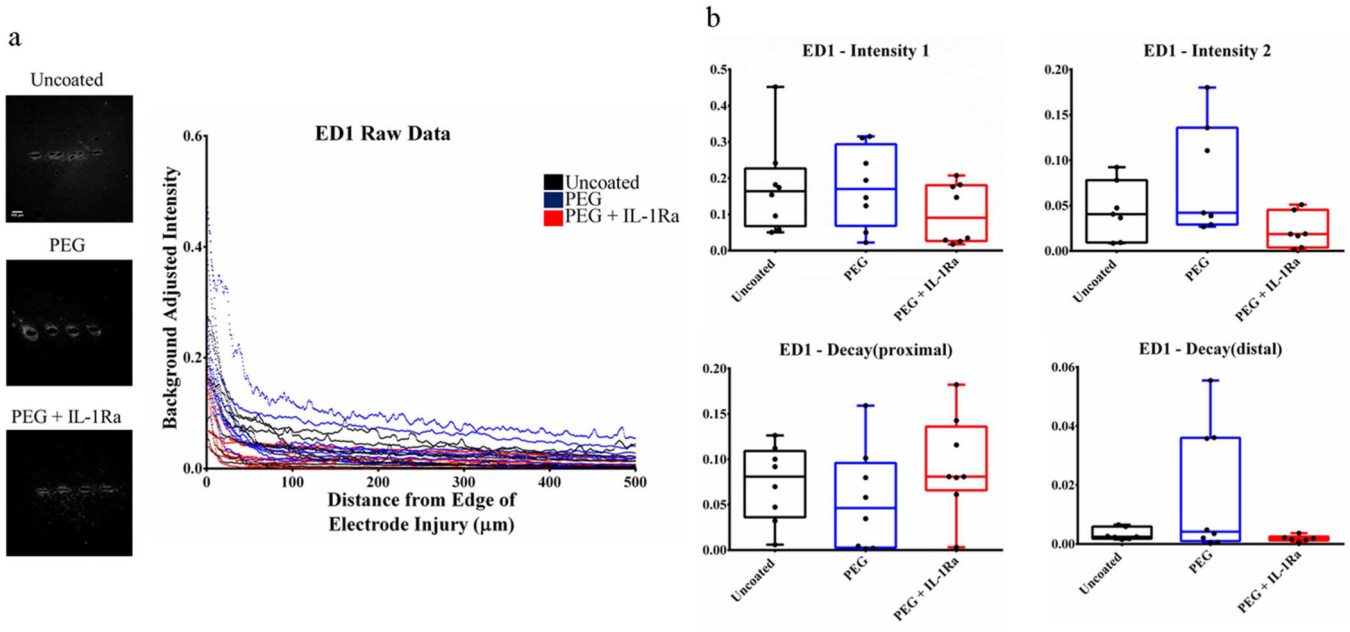

Figure 6.

Immunofluorescence analysis for activated microglia (ED1). (a) Immunofluorescence images (left) and corresponding intensity profile (right) for uncoated, PEG, and PEG +IL-1Ra (n=8 per group). (b) Parameter plots indicate differences in each parameter of Equation 1 for each group. The box plots indicate minimum, 25th percentile, median, 75th percentile, and maximum, with individual points shown for each sample.

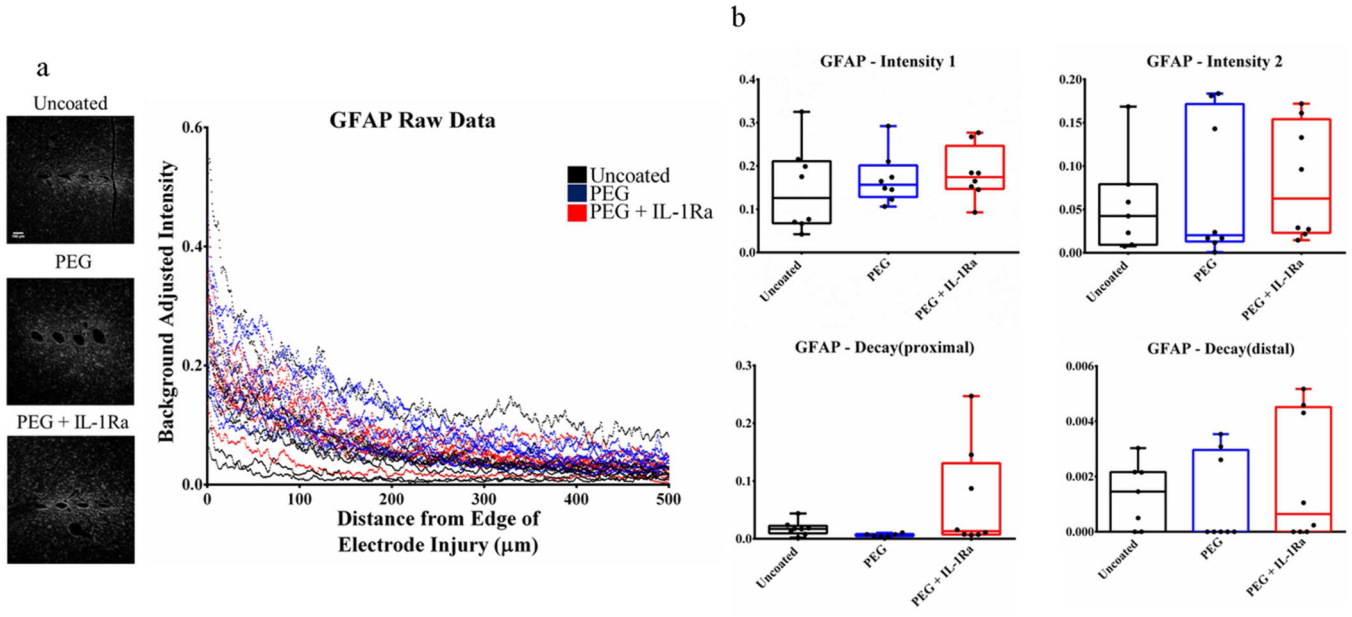

Figure 7.

Immunofluorescence analysis for glial fibrillary acidic protein (GFAP) for astrocytes. (a) Immunofluorescence images (left) and corresponding intensity scale (right) for uncoated, PEG, and PEG+IL-1Ra (n=8 per group). (b) Parameter plots indicate differences in each parameter of Equation 1 for each group. The box plots indicate minimum, 25th percentile, median, 75th percentile, and maximum, with individual points shown for each sample.

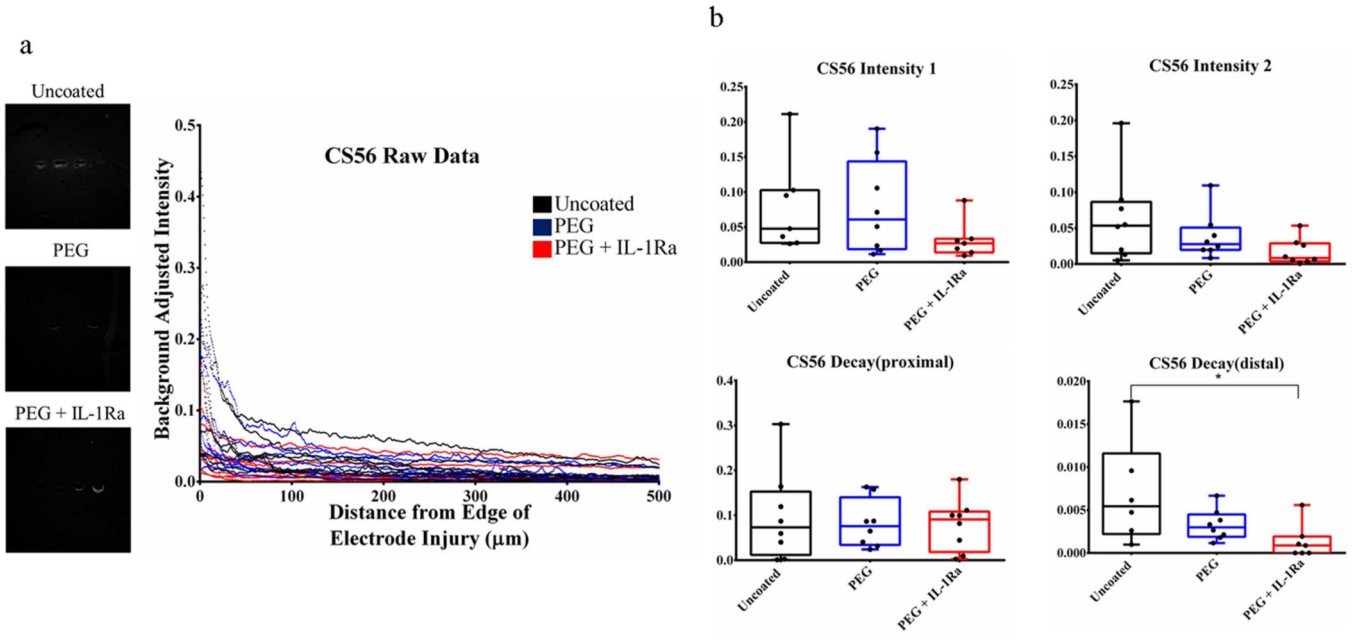

Figure 8.

Immunofluorescence analysis for chondroitin sulfate (CS56) for glycosaminoglycans at the injury site. The $Decay_{distal}$ parameter was significantly lower for PEG+IL-1Ra compared to uncoated samples. Other parameters were not significantly different. The box plots indicate minimum, 25th percentile, median, 75th percentile, and maximum, with individual points shown for each sample. * = $p < 0.05$.

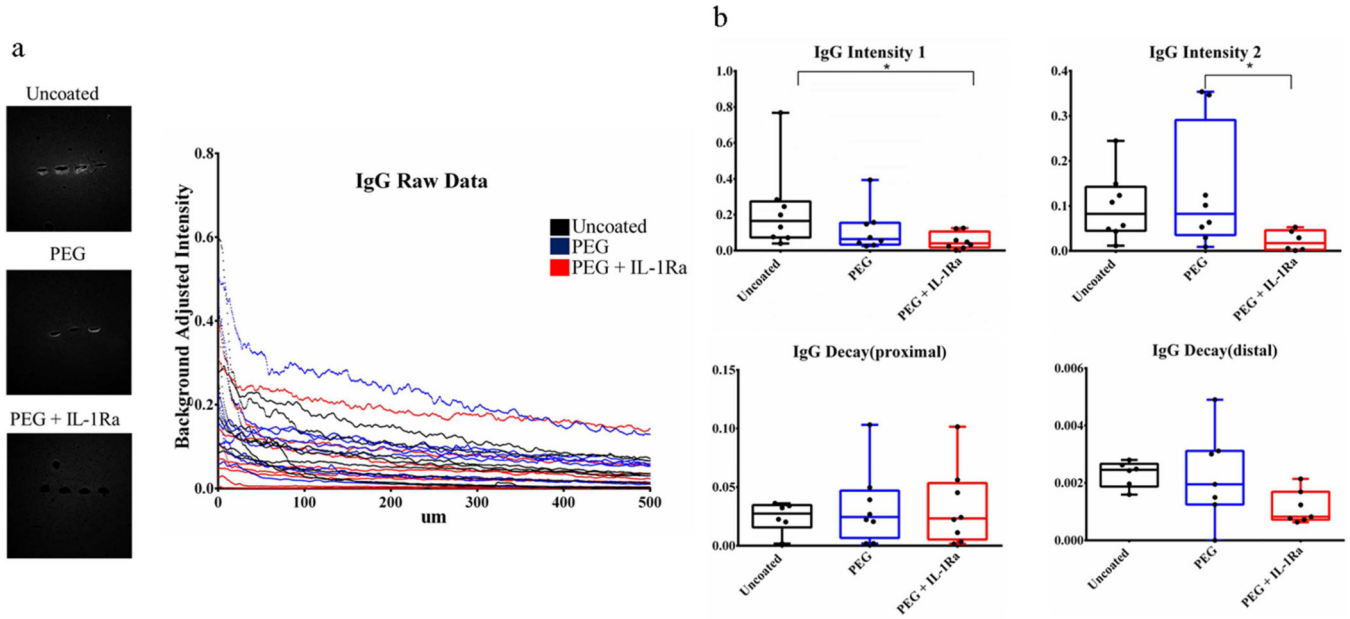

Figure 9.

Immunofluorescence analysis of rat IgG for blood brain barrier breach. The $Intesity_1$ parameter was significantly lower for PEG+IL-1Ra compared to uncoated samples. $Intensity_2$ was also significantly lower for PEG+IL-1Ra compared to PEG samples. Other parameters were not significantly different. The box plots indicate minimum, 25^{th} percentile, median, 75^{th} percentile, and maximum, with individual points shown for each sample. * = $p < 0.05$.

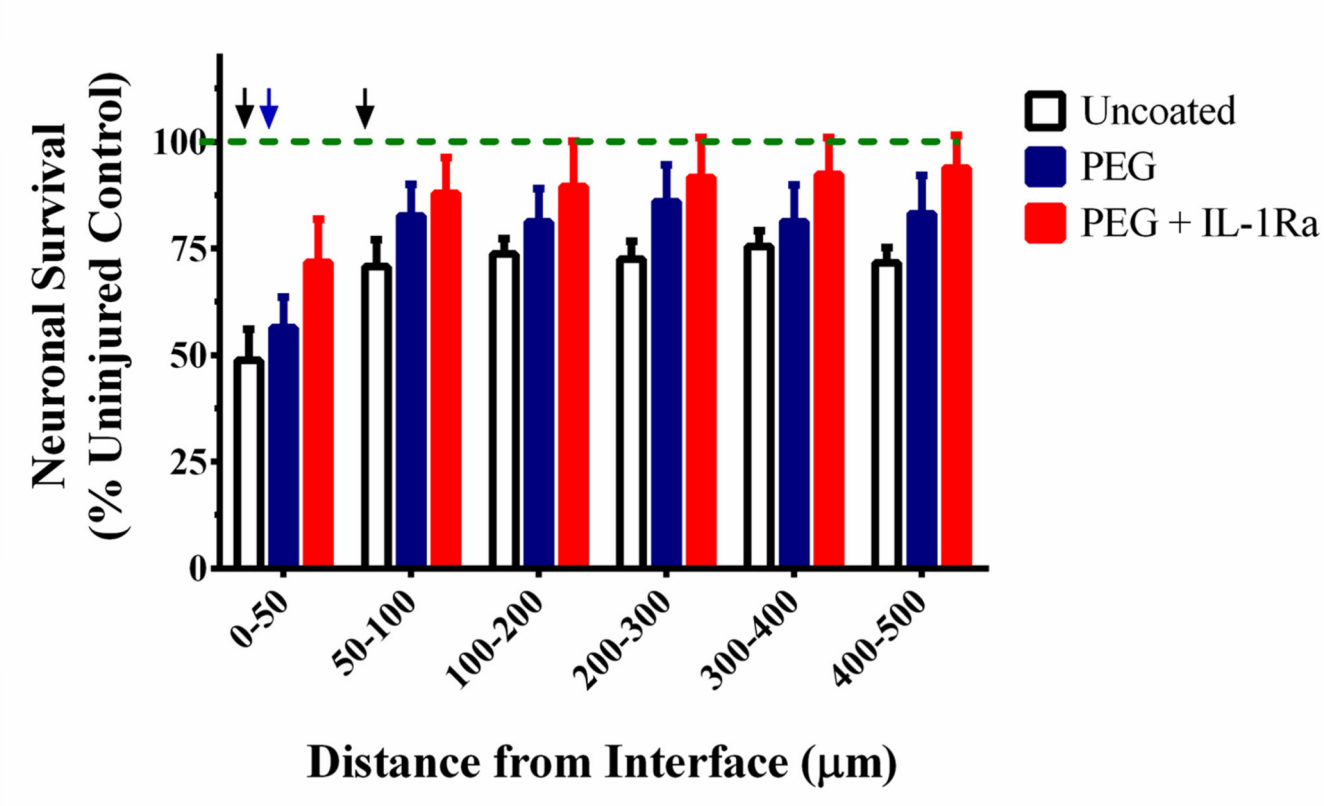

Figure 10.

Neuronal survival around the electrode. Uninjured control is indicated by the green dotted line. Black arrows indicate distances (0–50, 50–100 μm) at which uncoated samples were significantly lower than uninjured control ($p < 0.05$), whereas the blue arrow indicates distance (0–50 μm) at which PEG was different from uninjured control ($p < 0.05$). PEG +IL-1Ra was not significantly different from the uninjured control for any distance analyzed. At distances greater than 100 μm from the implant, all groups were equivalent to uninjured control.

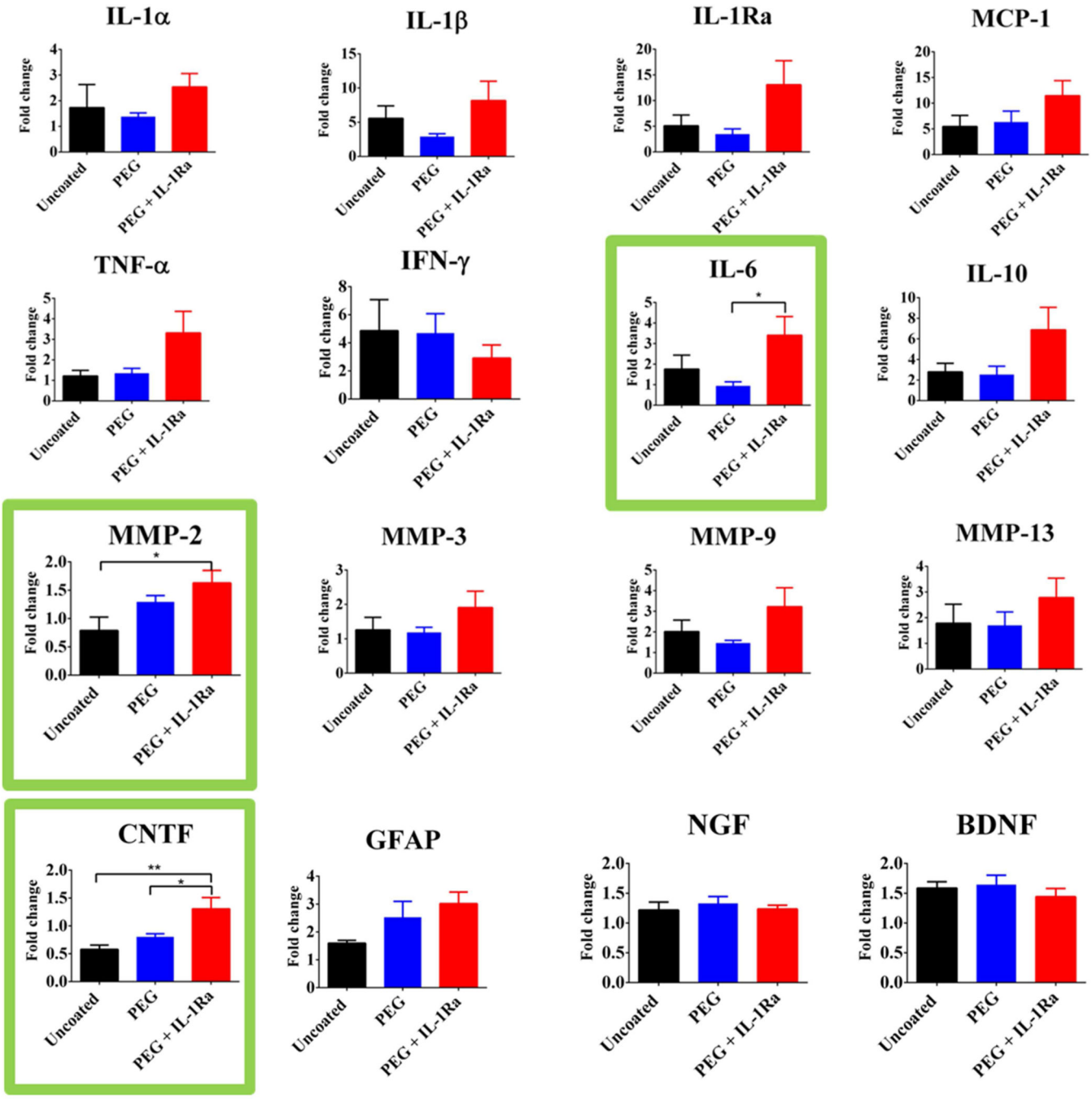

Figure 11.

Expression of inflammatory and neuronal survival genes at the implant site. Values represent fold-change over uninjured contralateral tissue. Genes with significant differences are outlined in green. * = $p<0.05$, ** = $p < 0.01$.

Table 1

Antibodies used for immunofluorescence analysis

Antibody	Supplier	Cell / Tissue Identified
Glial fibrillary acidic protein (GFAP)	Abcam ab7260	Astrocytes
NeuN	Millipore MAB377	Neuronal nuclei
OX42 / CD11b	Chemicon CBL1512	Resident microglia
ED1 / CD68	AbD Serotec MCA341R	Activated microglia
Alexa Fluor - Rat IgG	Life Technologies A11006	Blood brain barrier breach
CS56	Sigma C8035	Chondroitin sulfate

Table 1

Gene Targets for qRT-PCR Analysis

IL-1α	Interleukin - 1α	MMP-2	Matrix metalloproteinase – 2, 3, 9, 13
IL-1β	Interleukin - 1β	MMP-3	
IL-1Ra	Interleukin −1 receptor antagonist	MMP-9	
IL-6	Interleukin - 6	MMP-13	
IL-10	Interleukin - 10	NGF	Nerve growth factor
MCP-1	Monocyte chemoattractant protein - 1	BDNF	Brain derived neurotrophic factor
TNF-α	Tumor necrosis factor - α	CNTF	Ciliary neurotrophic factor
IFN-γ	Interferon-γ	GFAP	Glial fibrillary acidic protein